Journal of Engineering Science and Technology
Vol. 16, No. 3 (2021) 2378 - 2393

NUMERICAL INVESTIGATION OF CONJUGATE COMBINED CONVECTIVE HEAT TRANSFER FOR INTERNAL LAMINAR FLOW OF AL_2O_3/WATER NANOFLUID THROUGH TUBE – FLAT PLATE SOLAR COLLECTOR

MAHMOUD SH. MAHMOUD

Department of Mechanical engineering, Engineering College,
Al-Nahrain University, Baghdad, Iraq
Email: engmahmoud75@eng.nahrainuniv.edu.iq

Abstract

Investigating a 3D flat plate tube – sheet solar collector (FPSC) numerically using nanofluid (Al_2O_3/water) under the conditions as laminar, conjugate-mixed convective heat transfer. Ansys Fluent 2019R1 simulated the results for heat transfer fluid (HTF) inside a flat-plate tube – sheet solar collector for, Nusselt number, distribution of velocity and temperature, pressure drop entropy generation and friction factor, with the variation of the Richardson number from (0.5 to 7), laminar state, (Reynolds number < 2300), nanofluid concentration (1%, 2%, and 4%) and nano particle size (25 nm and 100 nm). In the present study, the effect of using nanofluid on the performance of the (FPSC) was investigated. It is concluded that using nanofluid, with (25 nm) size, at a constant Richardson number, a reduction in pressure drop rates is produced. The performance of the FPSC was increased by 84.35% at a volume fraction of 2 %.

Keywords: Conjugate, Combined convection, Internal flow, Laminar nanofluid, Solar collector, Tube-flat plate.

1. Introduction

Flat Plate Solar Collectors (FPSC) are a popular hot water supply mechanism and are located above residential or public buildings. Sunlight passes through one or two translucent glasses hitting the absorber layer, aluminium sheets were used. Solar energy heats the absorber plate and turns it to heating energy. The absorber plate is heated by heat transferred from the fluid to the tube [1-3]. When there is a temperature drop through the film layer of interaction between solids and fluids, it is known as conjugate heat transfer.

It was designed to simulate the optimal nanofluid profile for a fully developed flow in 3D FPSC. It was found that the Nusselt number is greater than that for the heat tube and less than 9% of the thermal efficiency; overall was found to be the most important variability between the experimental and numerical data [4].

While FPSCs have many benefits, such as sun-tracking and high reliability, their low thermal performance complicates their widespread use and development. Researchers have, however make use of various approaches to solve this significant inadequacy, notably contributing metallic or non-metallic nanoparticle sized with a range of 1 and 100 nm within the main functional FPSC geometry or fluid revision to achieve an optimal prototype that improves efficiency [5].

Using nanoparticles with water as the base fluid is widely used for heat transfer enhancement, Arjun and Rakesh [6], had studied the effect of using 23 nm average particle size of Al_2O_3/water with percent of volume concentration from (0-5) inside a micro channel. They compared between Re number effect on pressure drop and temperature. The achieved enhancement is approximately 83%.

The numerical investigation of a 2D square enclosure with a hop-heated side and conjugate laminar natural convection boundary conditions, they found the characteristics effect on the fluid flow and heat transfer behaviours. They stated that, concerning the fluid part, the average Nusselt number increases for a known wall thickness, with an increase in the thermal conductivity ratio and Rayleigh number [7].

Several previous studies and geometric parameters of the FPSC are listed here. The optimal inclination angle was confirmed between April and September at (10°) and between (30° and 35°) for the rest of the year. They also assessed the finest instantaneous efficiency of their collectors and a global heat loss factor of (85.1%) and (3.127%) respectively. It is simulated as a steady-state FPSC for plate thickness, tube spacing and length, layer thickness and tube diameter. Simulating a collector of relatively low bed height and a larger internal diameter could also improve system the performance [8].

FPSC were optimized using Al_2O_3 / water nanofluid, open and closed-loop exergy efficiency, while Iran's temporary climate, solar radiation, and ambient temperature were presumed inexplicable. They found that the relationship between each integrated variable and optimal exergy efficiency was linear. During power failure or times of low energy consumption, FPSC can achieve stagnation temperatures above (170 °C) which can threaten residents with excessive pressure. In addition, they analytically examined the characteristics of a U-shaped, three-dimensional, packaged solar collector. Their analysis reveals that the filled collector tube's heat efficiency is (6%) higher than copper fine.

They also suggested that the thermal performance of the filled collector use would be favourable, as the absorber tube temperature decreases by (40 ºC). Some essential elements limit the power of existing water-based solar panels combined with increased solar energy with radiation and because of the high temperature difference, heat loss increases [9]. Serale et al. [10] numerically investigated the material of a solar collector together with a phase change material (PCM) and thermal transmission fluids to propagate solar thermal collector performance. Tested the effect of forced convection heat transfer on Prandtl and Reynolds numbers in a conventional flat plate collector riser using aluminium/water nanofluid. The gained energy could be increased by (4–6)%. For the thermal panel, the quality of streamlines and heating lines was found to depend primarily on Re and Pr numbers. However, with an increase in Re value or a decrease in Pr number, collector usefulness, and domain absolute speed increase. Results show that this FPSC sheet-on- tube form is more appropriate than the often used regarding heat transfer and temperature outlet [11].

The performance of the FPSC could be improved by changing the pipe cross section, Rostami et al. [12] had used elliptic pipes instead of the circular pipes this had led to increase in the fluid outlet temperature which had increased the collector thermal efficiency.

The use of nanofluid has some advantages and disadvantages, the main advantage is to increase the thermo-fluid properties that will lead to enhance in the thermal performance, while the disadvantages could be categorized by the cost, maintenance, and hazards. The aim is to reach a nanofluid with higher thermal conductivity and low viscosity [13]. An important parameter in mixed convection heat transfer is Richardson number, where the heat transfer is proportional with Richardson number [14].

This manuscript was first modelled by a relatively new oblique 3D sheet-on-tube FPSC operating with the combined mixed laminar heat transfer mode, while HTF is selected to be aluminium oxide/water nano-fluid. The effect of nanofluid thermal-physical properties on the absorbed energy by FPSC, specifically nanoparticle size and volume concentration, Reynolds, Richardson, and Grashof numbers, are investigated carefully.

2. Problem Description

Figure 1 shows the geometric characteristics of the 3D FPSC sheet-on- tube used in complex mixed convection heat transfer in laminar region when applying uniform heat flux. It is a tube and an absorber plate length, width, thickness, and tube diameter are L=1.5 m, w=6 cm, and h=1 mm, and D=9 mm, respectively, define the copper-made stairway tube thickness and internal diameter d=0.5 mm.

The main computational domain is discretized up into multiple simple, small areas to improve grid sizes and mesh quality. Inlet and outlet zone: laminar nanofluid flow with constant initial temperatures is considered in the inlet zone with a well-grown velocity distribution, while outlet boundary conditions are prescribed in the outlet region. In addition, the grid density near the rising tube walls is high enough to adequately represent the thermal-hydraulic quality of all simulation cases in this study.

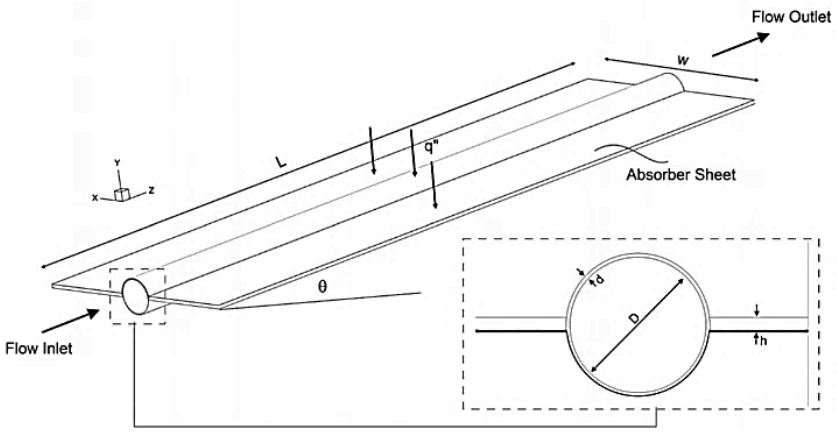

Fig. 1. Schematic configuration.

3. Mathematical Modelling

This article explores a 30º sheet-on- tube FPSC with relatively horizontal plane inclination under thoroughly mixed heat transfer. Working fluid at the riser inlet is considered to be the exact equivalent inlet with fully formed velocity distributor is selected as aluminium oxide nanofluid with different concentrations (0–4) % and (25–100) nm particle size. Using user-defined file (UDF), alumina, and water nanofluid properties have a series of temperature-dependent functions. It includes 3D, constant, Newtonian, and laminar flow. Uniform heat flux is applied to top surface of FPSC, prescribing non-slip, adiabatic for lateral plate absorber walls and lowering externally excessive tube. Gravitational force activates (*y*-axis) and directly (*z*-axis), body forces and pressure are neglected, including water and aluminium oxide nanoparticles, is assumed to have nil relative thermal balance [15]:

3.1. Governing equations

Continuity

$$\frac{\partial}{\partial x_i}(\rho u_i) = 0 \tag{1}$$

Momentum

$$\frac{\partial}{\partial x_j}(\rho u_i u_j) = \frac{\partial p}{\partial x_i} + \frac{\partial}{\partial x_j}(\nu(\frac{\partial u_i}{\partial x_j} + \frac{\partial u_j}{\partial x_i}) - u_i' u_j') \tag{2}$$

Energy

$$\frac{\partial \rho c_p u_j T}{\partial x_j} = \frac{\partial}{\partial x_j}(k\frac{\partial T}{\partial x_j} - \rho c_p \overline{u_j T}) + S_t \tag{3}$$

3.2. Thermo physical properties of nanofluid

Al_2O_3 water base nanofluid Thermo physical are listed below [13]:

Density,

$$\rho_{\mathrm{nf}} = (1-\phi)\rho_f + \phi\rho_p \tag{4}$$

The water density is

$$\rho_f = -3\times10^{-3}T_{\mathrm{avg}}^2 + 1.505T_{\mathrm{avg}} + 816.781 \tag{5}$$

where (T_{avg}) is the water average temperature in (K).

$$(\rho c_p)_{\mathrm{nf}} = (1-\phi)(\rho c_p)_f + \phi(\rho c_p)_p \tag{6}$$

$$c_{\mathrm{pf}} = -4.63\times10^{-5}T_{\mathrm{avg}}^3 + 0.0552T_{\mathrm{avg}}^2 - 20.86T_{\mathrm{avg}} + 6719.637 \tag{7}$$

$$\mu_{nf} = (123\phi^2 + 7.3\phi + 1)\mu_f \tag{8}$$

Water's viscosity is

$$\mu_f = 2.414\times10^{-5}\times10^{247.8/(T_{\mathrm{avg}}-140)} \tag{9}$$

Thermal conductivity is calculated as,

$$\frac{k_{nf}}{k_f} = \frac{k_p+(n-1)k_f-\phi(n-1)(k_f-k_p)}{k_p+(n-1)k_f+\phi(k_f-k_p)} + \frac{\rho_p\phi C_{p,p}}{2k_f}\sqrt{\frac{2\kappa T_{avg}}{3\pi d_p\mu_f}} \tag{10}$$

Water thermal conductivity can be determined from the relation:

$$k_f = 0.6067(-1.26523 + 3.704(\frac{T_{\mathrm{avg}}}{298.15}) - 1.43955(\frac{T_{\mathrm{avg}}}{298.15})^2) \tag{11}$$

3.3. Boundary conditions

Used boundary conditions for FPSC are as follow:

Inlet section,

$$u = v = 0, w = U_{\mathrm{inlet}}, T = T_{\mathrm{inlet}} \tag{12}$$

FPSC's upper surface,

$$u = v = w = 0$$

$$q_w'' = I(\lambda\kappa) - h(T_{\mathrm{col}} - T_{\mathrm{amb}}) \tag{13}$$

Thermal physical properties of Al_2O_3 (k =36 W/m.K, Cp=765 J/kg.K, and ρ = 3970 kg/m^3).

Adiabatic walls:

$$u = v = w = 0$$

$$\frac{\partial T}{\partial y} = 0 \tag{14}$$

Outlet tube section:

$$\frac{\partial u}{\partial z} = \frac{\partial v}{\partial z} = \frac{\partial w}{\partial z} = 0$$

$$\frac{\partial T}{\partial z} = 0 \tag{15}$$

Interfacing between the working fluid and the surface of the heating pipe,

$$k\frac{\partial T}{\partial x} = k_s\frac{\partial T_s}{\partial x} \tag{16}$$

The apparent friction factor,

$$f = \frac{2\Delta p}{\rho U_{inlet}^2}\frac{D_h}{L} \tag{17}$$

Nusselt number is,

$$\overline{Nu_z} = \frac{q_w'' D_h}{k(\overline{T_w}(z) - \overline{T_f}(z))} \tag{18}$$

$$\overline{T_w} = \frac{1}{2\pi}\int_0^{\pi} T_w(Z,\phi)d\theta \tag{19}$$

Thus, the convection heat transfer coefficient is,

$$h_{avg} = \frac{Nu \times k_{nf}}{D_h} \tag{20}$$

Thermal efficiency is given by,

$$\eta = \frac{Q_u}{A_a I} = \frac{\dot{m}c_p(T_{outlet} - T_{inlet})}{A_a I} \tag{21}$$

For the studied FPSC computational domain, obtaining the thermal performance and the heat generation as;

$$S''_{g,\,Total} = S''_{g,\Delta p} + S''_{g,\Delta T} \tag{22}$$

$$S''_{g,\Delta p} = \frac{\mu}{T}\left[\begin{array}{c} 2\times\left\{\left(\frac{\partial u}{\partial x}\right)^2 + \left(\frac{\partial v}{\partial y}\right)^2 + \left(\frac{\partial w}{\partial z}\right)^2\right\} \\ +\left(\frac{\partial u}{\partial y} + \frac{\partial v}{\partial x}\right)^2 + \left(\frac{\partial u}{\partial z} + \frac{\partial w}{\partial x}\right)^2 + \left(\frac{\partial v}{\partial z} + \frac{\partial w}{\partial y}\right)^2 \end{array}\right] \tag{23}$$

$$S''_{g,\Delta T} = \frac{k}{T^2}\left[\left(\frac{\partial T}{\partial x}\right)^2 + \left(\frac{\partial T}{\partial y}\right)^2 + \left(\frac{\partial T}{\partial z}\right)^2\right] \tag{24}$$

To find the enhancement value in performance, (r_s) can be defined as the ratio between nanofluid entropy generation and base fluid (water) entropy generation [16, 17]

$$r_s = \frac{(S''_{g,\,Total})_{nf}}{(S''_{g,\,Total})_f} \tag{25}$$

The following dimensionless group represent Reynolds, Prandtl, Grashof, and Richardson numbers.

$$Re = \frac{\rho U_{inlet} D_h}{\mu} \tag{26}$$

$$Pr = \left(\frac{C_p \mu}{k}\right) \tag{27}$$

$$Gr = \frac{g\beta q_w'' D_h^4}{k\nu^2} \tag{28}$$

$$Ri = \frac{Gr}{Re^2} \tag{29}$$

4. Grid generation, Independence and Validation.

FPSC sheet on tube and working nanofluid had been meshed by using ANSYSFLUENT 2019R1 with unstructured grid of tetrahedral element type. The number of grids is (5125479) cells as shown in Fig. 2. Six different cell numbers are used to test the effect of meshing number on results as shown in Table 1. To choose the finest mesh number, the percent error between the values of the corresponding parameters (average convection heat transfer coefficient ($h_{avg.}$), and friction factor (f)), will have the smallest value. Therefore, a mesh with perfect grids consists entirely of (12548300) cells being assigned in this work to perform all algorithmic analytics to mix the computational cost and ensure a high accuracy.

For mathematical modelling with high accuracy, numerical procedure validity, three different comparisons have been made with previous related experimental, theoretical, and numerical investigations concerning Nu, rate of generated entropy because of heat transfer, and friction factor through heating pipe. Using Al_2O_3/water nanofluid [5], a vertical copper tube of inner diameter 6.35 mm, and 2.24 m in length had been designed to work in laminar mixed convection with the same boundary conditions.

Table 1. Mesh independence, for Al_2O_3/water nanofluid with ϕ=1.5% is used at Re = 1500.

No. of elements	$h_{avg.}$ (W/m^2.K)	f
56454	806.0507	0.05493
88792	778.7838	0.0523
5125479	758.2937	0.05073
10189020	744.6603	0.04999
12548300	740.4051	0.04969
27334067	739.8644	0.04961

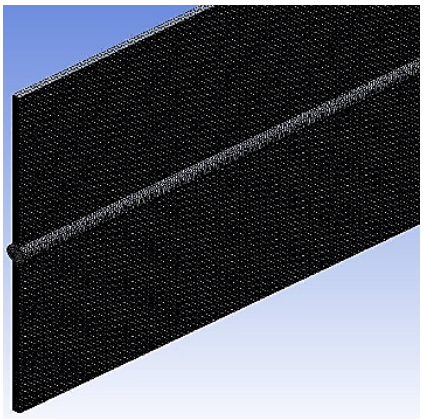

Fig. 2. Mesh generation of computational domain.

The validation between experimental results of [9, 18] correlation with obtained numerical results of the present study as shown in Fig. 3.

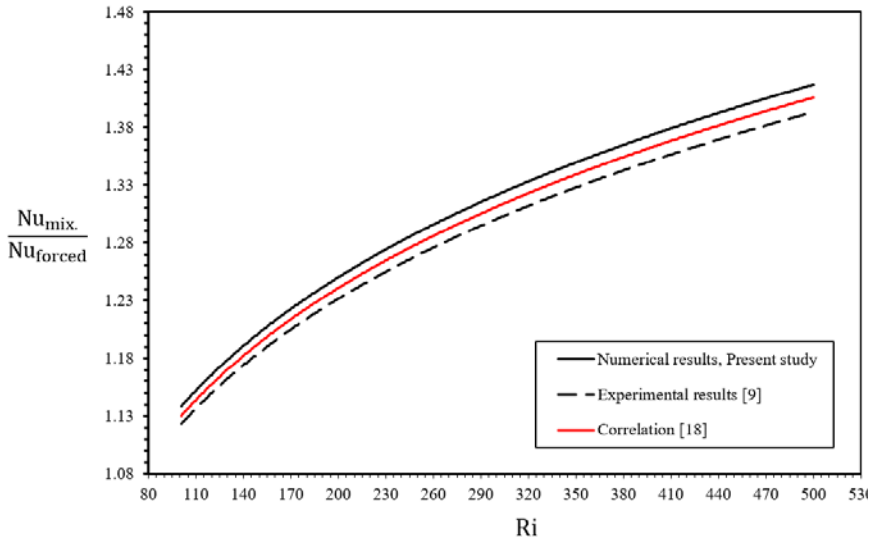

Fig. 3. Comparison between numerical results with that experimental results for [9, 18].

A 1-m length pipe with (6 mm) diameter operating incompressible flow, forced convective heat transfer was simulated to reassure entropy generation by heat transfer, while Al_2O_3 /water nanofluid concentration of (1%) was selected for HTF. As shown in Fig. 4, a reasonable agreement appears to exist between both Moghaddami et al. [18] and the highest variability between Moghaddami's et al. and present work data is 1.2%. Regarding the present numerical study, a correlation for Nusselt's number ratio is given by Eqn. (30).

$$\left(\frac{Nu_{mix.}}{Nu_{forced}}\right) = 0.606 * Ri^{0.1367} \tag{30}$$

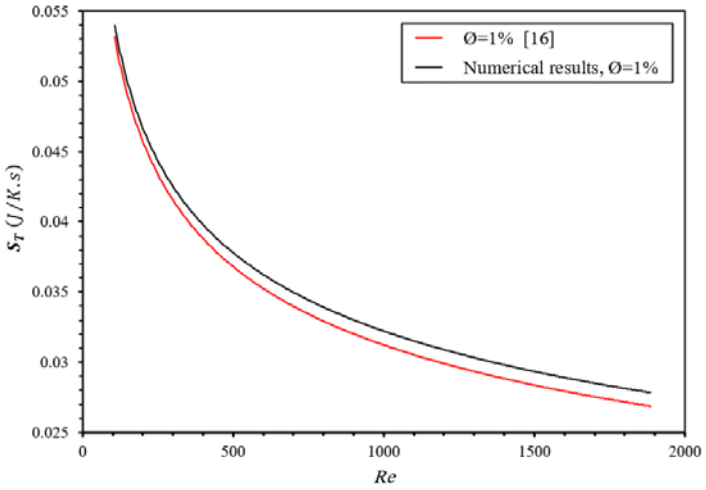

Fig. 4. Validation of the present numerical code with Moghaddami et al. [18].

4. Results and Discussion

Figure 5 shows effect of nanofluid volume concentration with respect to mass flow rate. Mass flow rate is inversely proportional with outlet temperature. Therefore, fluid flow through the absorber receives lower hot side heat relatively. The effectiveness increased with nanofluid concentration, the temperature at outlet section rises.

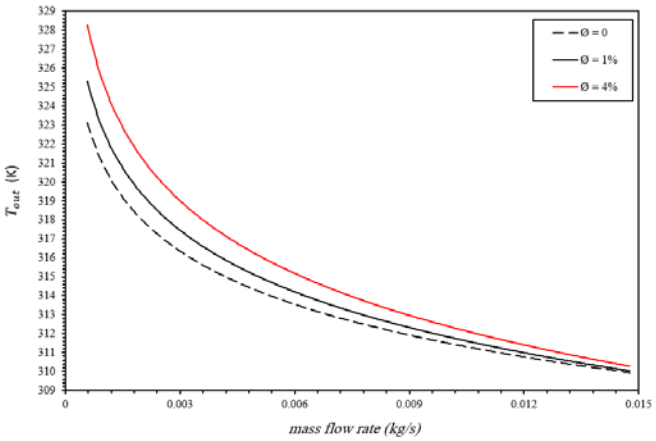

Fig. 5. Nanofluid outlet temperature changes at different Ø and $\dot{m}$.

Nusselt number variations at various volume fraction is clarified in Figs. 6(a) and 6(b), (Al_2O_3/water nanofluid) with variation for Reynolds numbers and Richardson numbers, for a specified nanoparticle diameter. As the nanoparticle volume fraction increases there is a decrease in Nusselt number, at a specified Richardson number. In this article, regarding the concerns of mixed convection, Nusselt number could be presented as a function of both Reynolds and Rayleigh numbers. As Richardson numbers began to grow at constant volume concentrations, the decreasing of Nusselt number was noticed. Richardson growth tends not merely to steadily increase in Rayleigh number, but also to decrease the Reynolds number by a certain volume concentration significantly. In the lower discharge the Richardson number slightly decreased, while nanofluid strengthened its growing strongly. This reduces the number of Nusselt by increasing the number of Richardson at a certain nanofluid concentration. Nusselt numbers are higher for 25 nm particles compared with 100 nm.

Such a trend is also described, considering both thermal conductivity and numerical concepts of Rayleigh. Thermal conductivity interacts with nanoparticles. it decreases as the diameter of nanoparticles increases, therefore the number of Rayleigh decreases. natural heat transfer effect in the riser decreases considerably with the decrease in Rayleigh number. When using higher nanoparticles, Nusselt 's number decreases. Figure 6(b), as particle concentration increases with Reynolds, Nusselt tends to decrease. As an adjusted number of Reynolds increases the concentration of nanofluid, there seem to be a decrease in the number of Rayleigh or swirl flow. Nusselt appears to be getting the lower number. At first glance, this result of lower Nusselt numbers and increased concentration of nanoparticles may seem intrinsic. It is significant to mention, even so, using nanoparticles with larger size reduces the natural heat transfer system in the laminar flow. Observing many past

studies [13], useful Al_2O_3/water nanofluid intensity increases with nanofluid concentration, decreasing fluid-induced dilution. The higher prevalence in heat transfer through the natural convection methodology would have been reversed, that cause decrease in Nusselt number. Significantly using nanofluid lead to enhance in Nusselt number at constant volume fraction and Reynolds number. Relatively high nanoparticles thermal conductivity is the main cause of poverty [19].

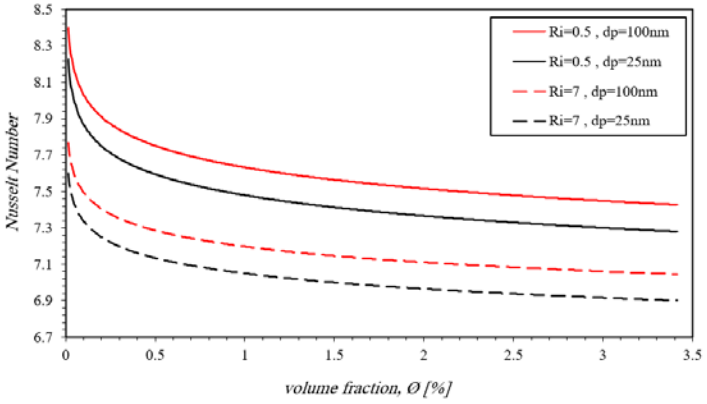

(a)

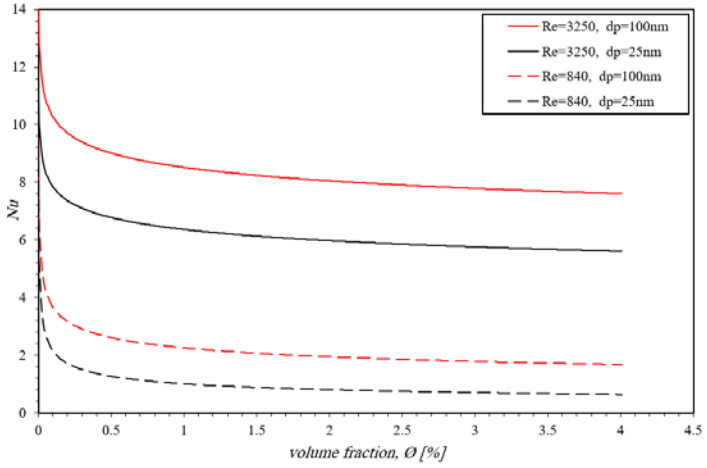

(b)

Fig. 6. Nusselt number trend for various volume fractions (ϕ) and nanoparticle size i.e., diameter for specified: (a) *Ri* and (b) *Re*.

The skin friction effects compared with volume concentration for Richards, Reynolds, and nanoparticles in parameters are shown in Figs. 7(a) and 7(b). As Fig. 7(a) illustrates the friction factor is increased up to a constant number of Richardson with the nanofluid volume fraction. The coefficient of friction has to do with an efficient density and suitable justification. The volume concentration of the set number of Richardson increases nanofluid active density leading to the improvement of friction factor. In addition, increased friction in a certain fraction of the density of Richardson. For instance, if the number of Richardson is increasing from (0.5 to 7),

the friction rate is nearly four times higher at any given volume concentration. Furthermore, at constant volume fraction an increase in the Richardson number cause reduction in the Reynolds number and thus the average speed also decreases, therefore, develops the friction. Finally, it has been found that the friction factor increased with larger nanoparticles. According to the data in Fig. 7(b), at certain Reynolds number, when nanoparticles volume fraction increased, the friction factor decreases. Expanding the weight percentage at a continual number of Reynolds reduces the mean velocity and active density of the fluid, also increase in volume fraction will cause decreases in friction factor. Raising the Reynolds number at an adjusted volume fraction also increases the friction coefficient because the riser increases the mean velocity. Predicated results shown in Fig. 7(b), it should also be mentioned that the friction factor is independent of the nanoparticles medium size.

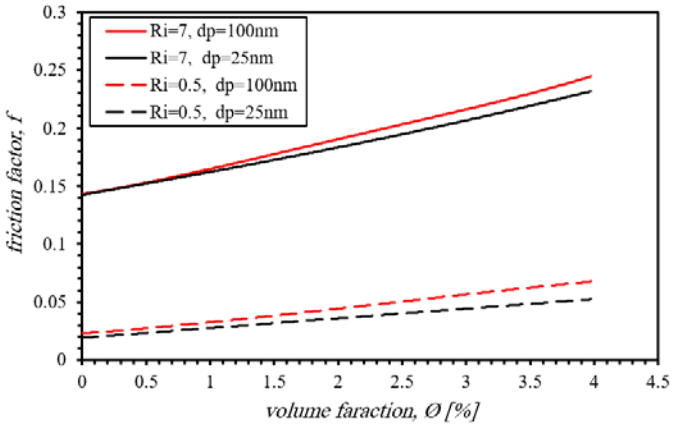

(a) Ri.

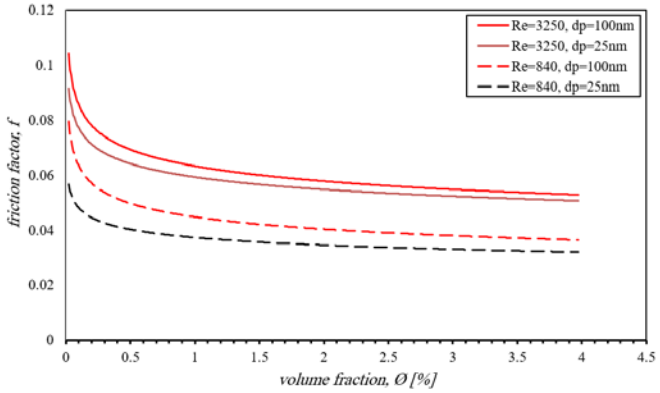

(b) Re

Fig. 7. Friction factor variations at various nanoparticle volume fraction and size for specified (a) Ri and (b) Re.

In Fig. 8 the relationship between the relative total nanofluid entropy to water rate for different Richardson numbers, and nanoparticles diameters are shown. The reverse relation of temperature to total viscous dissipation reduces entropy generation with more nanoparticle concentration. Lower Richardson number, increasing volume concentration which leads to entropy generation ratio increases marginally, then decreases at higher particle concentration, it also focuses on

temperature gradients. At lower Richardson number, though rising temperatures as the nanofluid volume percentage increases, the temperature gradients affect and entropy level increases. The ratio of total entropy generation decreases with more particle concentration while increasing the Richardson number at an adjusted volume concentration also results in the thermal entropy ratio increase. On the other hand, the entropy generation decreases as the nanofluid volume concentration increases and the thermal waste ratio increases with Reynolds number increases at a constant volume concentration. Increasing volume concentration at a fixed number of Reynolds tends to reduce bulk temperature, thus further increasing the total entropy generation ratio. The use of larger nanoparticles increases the viscous dissipation ratio by giving good thermal conductivity.

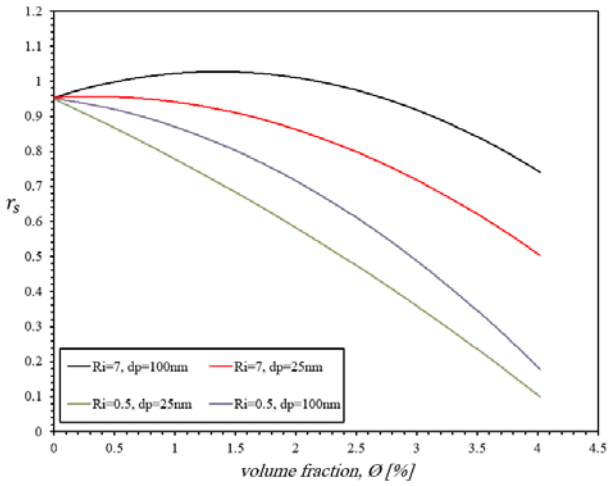

Fig. 8. Entropy generation ratio variations at various nanoparticle volume fractions and size for different (*Ri*).

In Fig. 9, shows the total thermal effectiveness for the studied FPSC versus nanofluid volume concentration for different *Re* numbers. As the nano-fluid volume fraction increases, total efficiency enhances at *Ø*=2% and then decreases. As far as Eqn. (21) is concerned, the temperature difference at an assigned volume concentration as the Reynolds increases. the overall efficiency increases when the concentration is less than 2% and it will be reversed after 2%. Furthermore, according to numerical simulation, the maximum nanofluid volume concentration where the system works effectively is 2%. However, it is important to note that perhaps the used FPSC sheet-on-tube produces significantly higher system efficiency than existing versions [20].

It was illustrated in Fig. 10 the validation for the numerical results and that from [18] and can be observed about a 1.2% difference. The effects on thermal field for two different nanofluid volume fractions are shown in Fig. 11. Within the riser the only thermal plume exists becomes less effective as the volume concentration increases. On the other hand, the mean bulk temperature of nanofluid decreases as the volume fraction increases, at a certain Reynolds number.

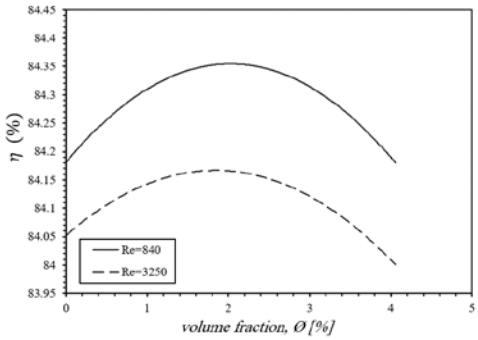

Fig. 9. Overall thermal efficiency variations for various volume fraction and Reynolds numbers for *dp*=25 nm.

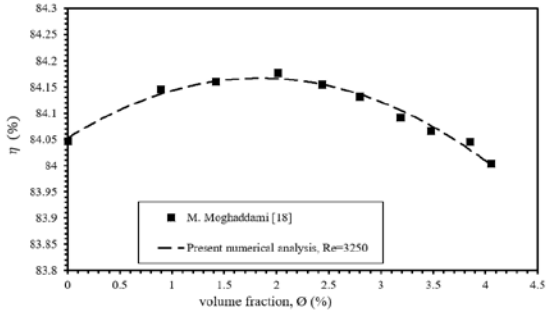

Fig. 10. Validation for the present numerical analysis with [18] at Re=3250.

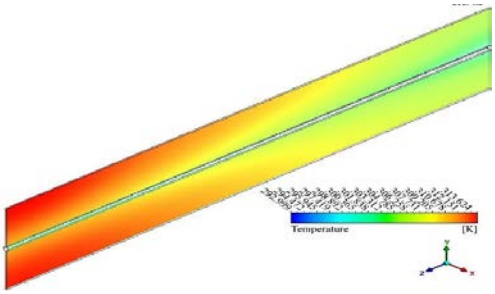

(a) Ø=1%.

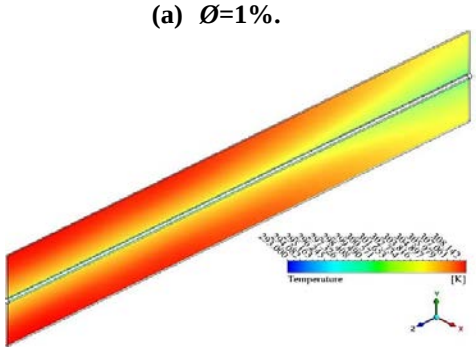

(b) Ø=4%.

Fig. 11. Volume fraction effect on (tube-on-sheet) temperature contours.

5. Conclusions

A numerical simulation was conducted using the ANSYS 2019R1 FLUENT commercial package for three-dimensional FPSC (tube-on-sheet) using water base nanofluid with a 30° inclination angle to the horizon. Laminar mixed convection conjugated heat transfer was considered, while water based (Al_2O_3) nanofluid at different volume concentrations and particle sizes was chosen as the working fluids, some important conclusions are summarized below:

- It is noticed that increase in Reynolds number causes a rise in Nusselt number, while it decreases with an increase in Richardson number and the nanofluid volume fraction.
- Al_2O_3 volume fraction has significant effect on the natural convection and prevents the existing of heat transfer in the downward direction.
- It is revealed that the heat transfer coefficient was increased between (45 and 58) % when compared with water.
- Pressure drop of working nanofluid through the tube in the FPSC system is inversely proportional with Richardson number.
- Using nanofluid with particle size of (25 nm) at a constant Richardson number produces reduction in pressure drop rates.
- The described FPSC design increased the performance by 84.35% at a volume fraction of 2 %.
- Future studies could include changing the nanofluid by using other materials or a composition of the base fluid in addition to flow type conditions.

Nomenclatures

A	Area, m^2
D_h	Hydraulic diameter, mm
d_p	Nanofluid particle diameter, nm
Gr	Grashof number
h	Convection heat transfer coefficient, $W/m^2.K$
I	Solar radiation on collector, W/m2
K	Thermal conductivity, W/m.K
L	Collector length, m
Nu	Nusselt number
P	Pressure, Pa
Pr	Prandtl number
q''_w	Heat flux, W/m^2
r_s	Entropy generation ratio
Re	Reynolds number
Ri	Richardson number
$S''_{g,\Delta p}$	Entropy generation due to friction, W/K
$S''_{g,\Delta T}$	Entropy generation due to temperature, W/K
$S''_{g,total}$	Total entropy generation rate, W/K
u, v, w	Velocity, m/s
W	Collector width, m

Greek Symbols

β	thermal expansion, 1/K
η	Thermal efficiency
μ	Viscosity, kg/m.s
ρ	Density, kg/m^3
$\emptyset$	Nanofluid volume concentration

Abbreviations

FPSC	Flat Plate Solar Collector
HTF	Heat Transfer Fluid
UDF	User Define File

References

1. Raboaca, M.S.; Goldanlou, A.S.; Rostami, S.; Sepehrirad, M.; Dezfulizadeh, A.; Hussein, A.K.; and Shadloo, M.S. (2019). Concentrating solar power technologies. *Energies*, 12(6), 2-17.
2. Mahmoud, S.; Abbas, A.; and Fakhrey, A. (2020). Solar parabolic trough collector tube heat transfer analysis with internal conical pin fins. *Journal of Green Engineering*, 10(10), 7422-7436.
3. Abbas, A.; Mahmoud, S.; and Fakhrey, A. (2020). Improvement of heat transfer for airflow through a solar air heater channel with cut-off desecrate baffles. *Journal of Green Engineering*, 10(7), 4292-4308.
4. Abdelkader, T.K.; Zhang, Y.; Gaballah, E.S.; Wang, S.; Wan, Q. and Fan, Q. (2020). Energy and exergy analysis of a flat-plate solar air heater coated with carbon nanotubes and cupric oxide nanoparticles embedded in black paint. *Journal of Cleaner Production*, 250, 119501.
5. Liao, Z.; and Faghri, A. (2016). Thermal analysis of a heat pipe solar central receiver for concentrated solar power tower. *Applied Thermal Engineering*, 102, 952-960.
6. Arjun, K.S.; and Rakesh, K. (2017). Heat transfer enhancement using alumina nanofluid in circular micro channel. *Journal of Engineering Science and Technology (JESTEC)*, 12(1), 265-279.
7. Belazizia, A. (2016). Conjugate natural convection in a two-dimensional enclosure with top heated vertical wall. *Journal of Engineering Science and Technology*, 11(10), 1373-1384.
8. Jiandong, Z.; Hanzhong, T.; and Susu C. (2015). Numerical simulation for structural parameters of flat-plate solar collector. *Solar Energy*, 117, 192-202.
9. Chen, Z.; Furbo, S.; Perers, B.; Fan, J.; and Andersen, E. (2012). Efficiencies of flat plate solar collectors at different flow rates. *Energy Procedia*, 30, 65-72.
10. Serale, G.; Goia, F.; and Perino, M. (2016). Numerical model and simulation of a solar thermal collector with slurry Phase Change Material (PCM) as the heat transfer fluid. *Solar energy*, 134, 429-444.
11. Kirmani, S.; Jamil, M.; and Rizwan, M. (2015). Empirical correlation of estimating global solar radiation using meteorological parameters, *International Journal of Sustainable Energy*, 34(5), 327-339.

12. Rostami, M.; Sepehrirad, S.; Dezfulizadeh, M.; Hussein, A.K.; Goldanlou, A.S.; and Shadloo, M.S. (2020). Exergy optimization of a solar collector in flat plate shape equipped with elliptical pipes filled with turbulent nanofluid flow: A study for thermal management. *Water*, 12(8), 2294-2310.
13. Khanafer, K.; and Vafai, K. (2018). A review on the applications of nanofluid in solar energy field. *Renewable Energy*, 123, 398-406.
14. Al-rashed, A.A.A.A.; Kalidasan, K.; Kolsi, L.; Velkennedy, R.; and Aydi, A. (2017). Mixed convection and entropy generation in a nanofluid filled cubical open cavity with a central isothermal block. *International Journal of Mechanical Sciences*, 135(12), 362-375.
15. Chacón, R.T.; and Lewandowski, R. (2014). *Mathematical and numerical foundations of turbulence models and applications. Modeling and simulation in science, engineering and technology*. New York: Springer.
16. Alsabery, A.I.; Gedik, E.; Chamkha, A.J.; and Hashim, I. (2020). Impacts of heated rotating inner cylinder and two-phase nanofluid model on entropy generation and mixed convection in a square cavity. *Heat and Mass Transfer*, 56(1), 321-338.
17. Khudheyer, A.F. (2020). Numerical investigation and exergetic analysis of convergent-divergent absorber tube in concentrated solar trough. *Journal of Green Engineering*, 10(10), 8083-8104.
18. Moghaddami, M.; Shahidi, S.; and Siavashi, M. (2012). Entropy generation analysis of nanofluid flow in turbulent and laminar regimes. *Journal of Computational and Theoretical Nanoscience*, 9(10), 1586-1595: American Scientific Publishers.
19. Hussein, A.K.; Walunj, A.; and Kolsi, L. (2016). Applications of nanotechnology to enhance the performance of the direct absorption solar collectors. *Journal of Thermal Engineering*, 2(1), 529-540.
20. Farshad, S.A.; and Sheikholeslami, M. (2019). Nanofluid flow inside a solar collector utilizing twisted tape considering exergy and entropy analysis. *Renewable Energy*, 141, 246-258.